Earth and Planetary Science Letters 303 (2011) 369–375

Contents lists available at ScienceDirect

Earth and Planetary Science Letters

journal homepage: www.elsevier.com/locate/epsl

Radial Q_μ structure of the lower mantle from teleseismic body-wave spectra

Yong Keun Hwang *, Jeroen Ritsema

Department of Geological Sciences, University of Michigan, Ann Arbor MI 48109, USA

ARTICLE INFO

Article history:
Received 11 August 2010
Received in revised form 19 January 2011
Accepted 23 January 2011
Available online 16 February 2011

Edited by: P. Shearer

Keywords:
Body waves
Attenuation
Lower mantle

ABSTRACT

We have measured 150,000 P and 130,000 S wave spectral ratios up to 0.8 Hz using recordings of 250 deep (focal depth >200 km) earthquakes from 890 global and regional network stations. We have inverted these data to estimate the attenuation parameters t^*_P and t^*_S for P and S waves and a radial profile of the quality factor Q_μ for the lower mantle. On average, t^*_P increases by about 0.2 s and t^*_S increases by about 0.7 s between epicentral distances of 30° and 97°. The relatively strong increase of t^*_S ($t_s \approx 4t^*_P$) suggests that intrinsic shear attenuation is the cause of the overall trend in our data. The increase of t^*_P and t^*_S with distance is smaller than predicted by models PREM [12], QL6 [11], and QLM9 [16]. Assuming PREM values for Q_μ in the upper mantle, where the data lack resolving power, the P and S wave spectra are explained best if Q_μ increases from about 360 at PREM's 670-km discontinuity to 670 in the lowermost mantle. The high values for Q_μ can be reconciled with previously determined values by invoking a frequency-dependence of $Q_\mu(\omega)$ that is proportional to $\omega^{0.1}$. Data that are separated in 'Pacific' and 'circum-Pacific' subsets have slightly different trends. Estimates of t^*_P and t^*_S for the Pacific data, which sample the large low shear-velocity province of the Pacific, are higher than the circum-Pacific estimates. Thus, it appears that the Pacific large low shear velocity province has accompanying low Q_μ. The difference in Q_μ in the lowermost 1000 km of the mantle beneath the Pacific and beneath the circum-Pacific is at most 17%. Lateral variations of this magnitude are marginally resolvable given the uncertainties of our measurements.

1. Introduction

Although seismic constraints of the mantle have come primarily from studies on elastic velocities, it is well recognized that joint interpretations of seismic velocities and attenuation are critical for understanding the structure and dynamical state of the Earth's interior.

Global variations of attenuation in the upper mantle have been estimated using both surface waves (Billien et al., 2000; Dalton et al., 2008; Gung and Romanowicz, 2004; Romanowicz, 1995; Selby and Woodhouse, 2002) and body waves (e.g., Bhattacharyya et al., 1996; Reid et al., 2001; Warren and Shearer, 2002). These global-scale studies are consistent with regional-scale studies (Baqer and Mitchell, 1998; Hwang et al., 2009; Lawrence et al., 2006; Roth et al., 2000; Sheehan and Solomon, 1992) and indicate that the upper 200–300 km of the mantle beneath oceans and tectonically active regions is generally more attenuating than the mantle beneath stable, continental shields.

Except for the study by (Lawrence and Wysession, 2006b), wave attenuation in the lower mantle has been modeled using 1D profiles (Fig. 1). Whole-mantle profiles, constrained by normal-modes (Durek and Ekström, 1996; Dziewonski and Anderson, 1981; Resovsky et al., 2005; Roult and Clévédé, 2000; Widmer et al., 1991) and ScS/S waveforms (Lawrence and Wysession, 2006a), have a common low Q_μ layer in the uppermost mantle (80–200 km depth), intermediate Q_μ values in the transition zone (200–650 km), and the highest Q_μ values in the lower mantle. However, absolute values of Q_μ and the depth dependence of Q_μ in the lower mantle differ in these profiles. PREM (Dziewonski and Anderson, 1981) and QL6 (Durek and Ekström, 1996) indicate constant values of 312 and 355 in the lower mantle, respectively. (Oki and Shearer, 2008) resolve lower mantle Q_μ value of about 620 using S–P ratio method at short-period band (3–10 s). (Resovsky et al., 2005) constrain Q_μ to decrease in the lowermost 1000 km of the mantle. Q_μ in PAR3P (Okal and Jo, 1990) and QM1 (Widmer et al., 1991) decrease throughout the lower mantle while it increases in the lower 1000 km of the lower mantle in model QLM9 (Lawrence and Wysession, 2006a). The study of (Warren and Shearer, 2000) provide a high-frequency (0.16–0.86 Hz) estimate of Q_P from global P to PP spectra. Their frequency-independent Q_P is about 2600 in the lower mantle which is more than three times larger than the Q_P value of 780 in PREM. Variable approaches, data sets and measurement uncertainties are responsible for these differences and underscore that the basic radial structure of Q is still poorly constrained.

In this study, we follow a classical approach in which Q is determined from the epicentral distance variation of the body-wave

* Corresponding author. Tel.: +1 734 763 4069; fax: +1 734 763 4690.
E-mail addresses: ykhwang@umich.edu (Y.K. Hwang), jritsema@umich.edu (J. Ritsema).

0012-821X/$ – see front matter © 2011 Elsevier B.V. All rights reserved.
doi:10.1016/j.epsl.2011.01.023

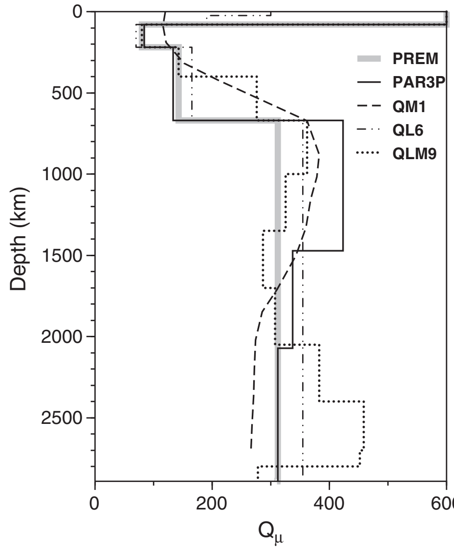

Fig. 1. Radial Q_μ structures of (thick grey line) PREM (Dziewonski and Anderson, 1981), (solid black line) PAR3P (Okal and Jo, 1990), (dashed line) QM1 (Widmer et al., 1991), (two-dot chain line) QL6 (Durek and Ekström, 1996), and (dashed dotted) QLM9 (Lawrence and Wysession, 2006a).

attenuation parameters t_P^* and t_S^*. The original study by (Teng, 1968) and subsequent studies of spectral ratios (e.g., Der and McElfresh, 1977; Der et al., 1982); (Solomon and Toksöz, 1970) and amplitude decay (e.g., Booth et al., 1974; Butler and Ruff, 1980) were mostly applied to band-limited, analog waveform data from the United States. Here, we measure t_P^* and t_S^* from a nearly two-decade long collection of digital waveforms from broadband seismic stations in regional and global networks. We describe our data in Section 2. We review methods and describe the epicentral variation of t_P^* and t_S^* and the inferred radial variation of Q_μ in Sections 3 and 4, respectively. Final conclusions are drawn in Section 5.

2. Data

2.1. Teleseismic body-wave spectra

The attenuation parameter t^* is defined as the ratio of the body-wave travel time t and the quality factor Q integrated along the ray path (e.g., Stein and Wysession, 2003):

$$t^* = \int_{\text{ray}} \frac{dt}{Q}. \tag{1}$$

We use t_P^* and t_S^* and Q_P and Q_μ to denote the attenuation parameters and quality factors of P and S waves, respectively. Since the amplitude spectrum of a body wave is proportional to the attenuation function $\exp(-\frac{1}{2}\omega t^*)$, the ratio $R_{ij}(\omega)$ of spectra $O_i(\omega)$ and $O_j(\omega)$ for the same earthquake is related linearly to the t^* difference recorded at stations i and j (Teng, 1968):

$$\ln R_{ij}(\omega) = -\frac{\omega}{2}\Delta t_{ij}^*. \tag{2}$$

While we have previously investigated spectral ratios of P waves to map lateral variation of t_P^* (Hwang et al., 2009), we study here the variation of t_P^* and new measurements of t_S^* as a function of epicentral distance. If Δ_i and Δ_j are the epicentral distances of stations i and j, we associate

$$\Delta t_{ij}^* = t_{\Delta_i}^* - t_{\Delta_j}^* \tag{3}$$

to depth-dependent attenuation in the lower mantle, using the fact that P and S wave turning depths increase monotonously with epicentral distance (Fig. 2). Q_μ is related to Q_P by

$$Q_P^{-1} = LQ_\mu^{-1} + (1-L)Q_\kappa^{-1}, \tag{4}$$

where $L = \frac{4}{3}(V_S/V_P)^2$ and V_S and V_P are the S and P wave velocities (e.g., Anderson and Given, 1982). If shear attenuation is much larger than bulk attenuation (i.e., $Q_\mu \ll Q_\kappa$), then

$$Q_P^{-1} = LQ_\mu^{-1}. \tag{5}$$

Eq. (5) predicts that t_P^* and t_S^* differ by about a factor of 4.5 and that the Q_P/Q_μ ratio is 2.25 (depending on the velocity structure of the mantle) which is almost the same as the Q_P/Q_μ ratio of 2.27 estimated in this study.

2.2. Measurements

We measure Δt^* using more than 150,000 P wave and 130,000 S wave spectral ratios from about 250 events with magnitudes larger than 6. The events occurred between 1987 and 2005 and have been recorded by broadband seismometers from global (GSN and Geoscope) and numerous regional networks. The focal depths of the earthquakes are larger than 200 km so that the P and S signals are not complicated by surface reflections (i.e., pP, sP, sS) and not attenuated strongly by the uppermost mantle in the source region. We limit the analysis to epicentral distances larger than 30° to avoid waveform complexity due to strong velocity gradients in the upper mantle and to distances smaller than 97° to avoid the effects of diffraction along the core. A high-pass filter with a corner frequency of 120 s is applied to the vertical-component P wave and the transverse-component S wave.

We inspect all waveforms to ensure that the signals are well above noise level, and have low-amplitude coda and impulse onsets. Typically, P-wave and S-wave time windows are about 8 s and 27 s long, respectively. However, we adjust these to isolate waveforms with similar characteristics. We measure Δt^* for pairs of stations that have similar source azimuths to minimize the effects of rupture directivity on the spectra. Examples of waveforms and spectral ratios have been shown by (Hwang et al., 2009). The amplitude spectra are estimated up to 0.8 Hz using the multiple-taper spectral analysis of (Lees and Park, 1995). Δt^* and its uncertainty are estimated by linear regression.

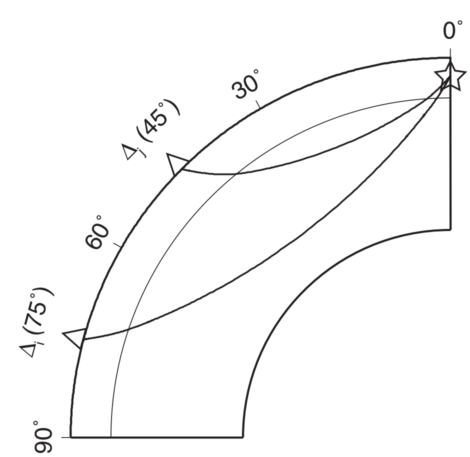

Fig. 2. Geometrical ray paths of P waves from a (star) 300-km deep earthquake source to (triangles) stations at epicentral distances of Δ = 45° and Δ = 75°.

Δt^* incorporates the effect of lateral variation in t^*, the influence of heterogeneity in the crust and mantle, scattering, and station 'site effects'. In addition, measurement errors in Δt^* arise due to the unstable nature of spectral ratios. Nevertheless, a signal of intrinsic attenuation is evident in our data when we plot Δt^* as a function of inter-station distance d $\Delta_{ij} = |\Delta_i - \Delta_j|$ (Fig. 3). Two aspects characterize intrinsic attenuation. First, the weighted average values of Δt^*_{ij} increase smoothly with increasing d Δ up to at least 45°. Second, the increase of Δt^*_S is about four times stronger than the increase of Δt^*_P. This is consistent with Eq. (5) and the ratio between t^*_P (~1 s) and t^*_S (4 s) estimated from spectral and time-domain body-wave studies (e.g., (Cormier, 1982)).

3. Distance variation of attenuation parameters

We estimate t^*_P and t^*_S at evenly spaced (1°) epicentral distances between $\Delta = 30°$ and $\Delta = 97°$ by solving three sets of equations. First, we relate a measurement of Δt^*_{ij} to the difference of t^* for a pair of stations i and j at epicentral distances Δ_i and Δ_j:

$$w^1_{ij}\left(t^*_{\Delta_i} - t^*_{\Delta_j}\right) = w^1_{ij}\Delta t^*_{ij}. \tag{6}$$

Eq. (6) is multiplied by a factor w^1_{ij}, which is determined by the 2σ uncertainty (ε_{ij}) of the measurement of Δt^*_{ij}:

$$w^1_{ij} = \exp\left\{-\left(\frac{\varepsilon_{ij}}{0.3}\right)^2\right\}. \tag{7}$$

Thus, Δt^* measurements with ε_{ij} larger than 0.3 s are weighed less than 1/e. Second, we impose the epicentral distance variation of t^* to be smooth:

$$w^2_{ij}\left(t^*_{\Delta_i} - t^*_{\Delta_j}\right) = 0, \tag{8}$$

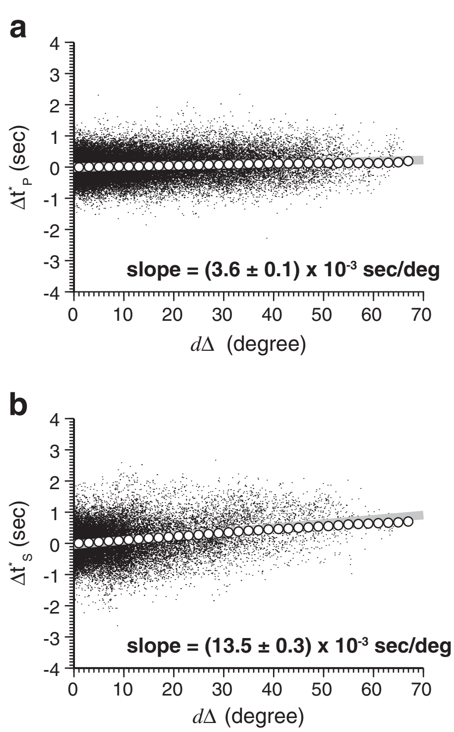

Fig. 3. (a) Δt^*_P and (b) Δt^*_S as a function of inter-station distance d Δ_{ij} ($= |\Delta_i - \Delta_j|$). Thick grey lines are best-fitting lines to the entire Δt^*_P and Δt^*_S data sets. Their slopes and 95% confidence ranges are indicated at the bottom. Circles are mean (a) Δt^*_P and (b) Δt^*_S values predicted from the epicentral variations of t^*_P and t^*_S for the global data, respectively in Fig. 4a and b.

where the weight is

$$w^2_{ij} = \exp\left\{-\left(\frac{d\Delta_{ij}}{5^\circ}\right)^2\right\}. \tag{9}$$

Third, we set the average value of t^* to be zero,

$$t^*_{30^\circ} + t^*_{31^\circ} + \ldots + t^*_{97^\circ} = 0, \tag{10}$$

since absolute values of t^* cannot be constrained from Δt^* measurements. The linear Eqs. (6), (8), and (10) can be written in matrix-vector form as $\mathbf{Gm} = \mathbf{d}$, where the elements of m are the t^* values at the 68 epicentral distances:

$$\mathbf{m} = \left(t^*_{30^\circ}, t^*_{31^\circ}, \cdots, t^*_{97^\circ}\right). \tag{11}$$

We estimate m by least-squares inversion.

3.1. Global variations of t^*_P and t^*_S

Since Δt^* are measurements derived from spectral ratios, we cannot constrain the absolute values of t^*_P and t^*_S. We plot our estimates of t^*_P and t^*_S in Fig. 4 setting $t^*_P =$ 0.7 s and $t^*_S =$ 3.0 s at $\Delta = 30°$, as predicted by PREM, to facilitate a comparison with predicted t^* values for the Q_μ profiles of PREM, QL6, and QLM9.

The large uncertainties and scatter in Δt^* results in wide error bars of t^*_P and t^*_S. Since the peaks and troughs are smaller than the error bounds, we emphasize only the general trend of t^*_P and t^*_S. We resolve an increase of about 0.2 s in t^*_P and about 0.7 s in t^*_S between 30° and 97°. Over this distance range, the increase in t^*_S is about 4 times stronger than in t^*_P.

The PREM, QL6, and QLM9 values are calculated using Eq. (1). For QL6 and QLM9, which provide only Q_μ, we relate Q_μ to Q_P using Eq. (5) and the P and S wave velocities of PREM. t^*_P and t^*_S inferred from our body-wave spectra increase more slowly with epicentral distance than t^*_P and t^*_S calculated for the published profiles. For PREM, QL6, and QLM9, t^*_P increases by about 0.4 s between 30° and 97° while our data indicate an increase of about 0.2 s (Fig. 4a). PREM and QL6, which have constant Q_μ values in the lower mantle (312 and 355, respectively) predict an increase of t^*_S of about 2.3 s and 2.0 s, respectively, between 30° and 97° (Fig. 4b). For the same distance range, t^*_S inferred from our body-wave spectra increases by only about 0.7 s. These differences indicate that the teleseismic body-waves experience less attenuation and that body-wave spectra are explained better by Q_μ values in the lower mantle that increase with depth.

The t^*_P and t^*_S curves for model QLM9 have kinks near $\Delta = 75°$. The reduction of the slopes for distances larger than 75° is due to the increase in Q_μ at depths larger than about 2050 km (Fig. 6). Since t^*_P and t^*_S predicted from QLM9 between about 75° and 95° are parallel to our t^*_P and t^*_S curves, the Q_μ structure of QLM9 below 2050 km depth is compatible with our body-wave spectra.

3.2. Pacific and circum-Pacific t^*_P and t^*_S variations

To determine whether lateral variations of attenuation in the lower mantle can be detected in our data, we analyze t^*_P and t^*_S for 'Pacific' and 'circum-Pacific' subsets of body-wave spectra (Fig. 5). These subsets are chosen using tomographic maps of shear velocity in the lower mantle (Ritsema et al., 1999). For the Pacific subset, P and S wave turning points are located in the lower mantle beneath the Pacific Ocean, where shear velocities are relatively low. The circum-Pacific P and S waves turn in the lower mantle where the shear velocity is relatively high. Thus, we estimate whether lateral variations in t^*_P and t^*_S, as determined by P and S wave turning points, correlate with the large-scale shear velocity variation of the lower mantle.

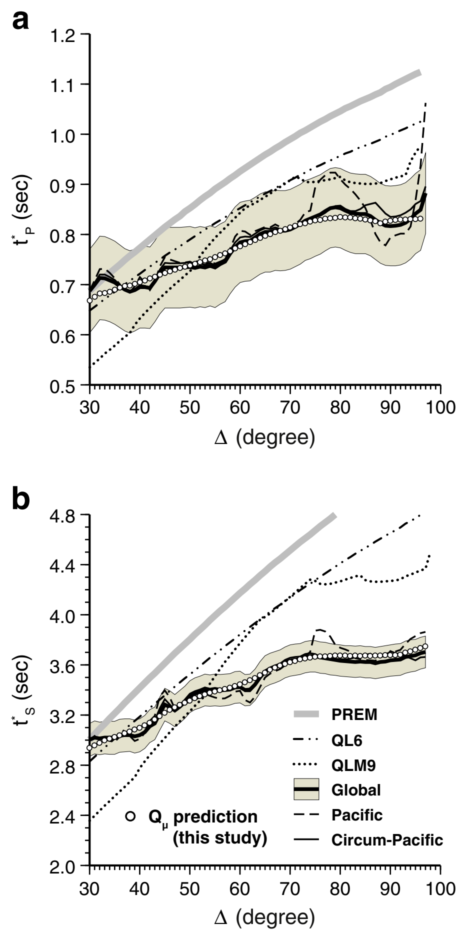

Fig. 4. Epicentral distance variations of (a) t_P^* and (b) t_S^* for the complete (global) data set (thick black lines) with their errors (shaded area), for the Pacific subset (dashed lines), and the circum-Pacific subset (thin black lines) at distances between 30° and 97°. Errors are determined from the uncertainties in the Δt^* measurements. t^* variations calculated from PREM (thick grey lines), QL6 (two-dot chain lines), and QLM9 (dashed dotted lines) at distances between 30° and 97° are plotted for comparison. t_P^* of PREM, QL6, and QLM9 are computed using Q_P structures converted from Q_μ profiles of PREM, QL6, and QLM9 using Eq. (5). Also shown are (a) t_P^* and (b) t_S^* variations predicted from our global Q_P and Q_μ models (white circles).

We can only constrain the difference between the Pacific and circum-Pacific subsets for epicentral distances between about 70° and 85° where both the Pacific and circum Pacific subsets are sufficiently large. This distance range corresponds to P and S turning depths of 1870–2470 km (layer 2 in Fig. 5). At distances smaller than 70°, corresponding to turning depths smaller than 1870 km (layer 1 in Fig. 5), fewer than 5% of the P and S waves turn below the Pacific Ocean. Therefore, the Pacific and circum-Pacific subsets include all spectral ratios for epicentral distances smaller than 70°. For epicentral distances larger than 85°, corresponding to turning depths larger than 2470 km (layer 3 in Fig. 5), P and S waves may interfere with CMB reflection phases (PcP and ScS) and render the measurements of spectral ratios inaccurate.

In Fig. 4, variations in t_P^* and t_S^* for the complete ('global') data set are compared with variations for the Pacific and the circum-Pacific subsets. t_P^* and t_S^* values for both subsets are smaller than PREM predicted t^* values at almost all epicentral distances. Global t_P^* and t_S^* values are most similar to the circum-Pacific values because the total number of measurements for the circum-Pacific group is about four times larger than the number of measurements for the Pacific group. For $\Delta > 70°$, Pacific t_P^* (0.86 s on average) and t_S^* (3.73 s on average) are larger than the circum-Pacific t_P^* (0.85 s on average) and t_S^* (3.67 on average) values. Although averages of t_P^* (0.84 s) and t_S^* (3.65) for the global data set are similar to circum-Pacific group t^* averages, the variation with distance is similar to the variation of the Pacific t^* within this distance range. Thus it appears that the relatively high Pacific t^* values are associated with the large low velocity anomaly beneath the Pacific Ocean. However, for Δ between 85° and 92°, the Pacific t_P^* values (0.80 s on average) are smaller than the circum-Pacific group t_P^* (0.85 s on average). This may indicate that P waves are not affected by a large low velocity province beneath the Pacific Ocean or that the P spectral ratios are contaminated by the PcP core reflection.

4. Radial variation of Q_μ

Given that t_P^* is lower than t_S^* by roughly a factor of four, we jointly invert the t_P^* and t_S^* for a profile of Q_μ. Q_μ in the lower mantle is parametrized using 22 layers with a uniform thickness of 100 km in which Q_μ is constant. Thus, Eq. (1) is written as

$$\sum_{n=4}^{N=25} \frac{t_n}{Q_\mu^n} = t^*, \tag{12}$$

where t_n and Q_μ^n are the travel time and quality factor in the n^{th} layer of the lower mantle, respectively. Since the absolute values of t_P^* and t_S^* are unconstrained by our spectral ratios and since teleseismic body-waves propagate vertically through the upper mantle, we assume that Q_μ in the upper mantle (depth < 770 km) is described by PREM:

$$\frac{Q_n^{\mathrm{PREM}}}{Q_\mu^n} = 1, \tag{13}$$

where Q_n^{PREM} is the Q_μ value of PREM in the n^{th} (n = 1, 2, and 3) layer of the upper mantle. Q_μ in the best-fitting profile decreases by less than 10% and only in the upper part of the lower mantle (< 1270 km depth) if model QLM9, which differs most from PREM in the upper mantle, is used to constrain the upper mantle Q_μ structure.

For S waves, we use t_S^* and compute S wave travel times and ray paths using PREM. For P waves, we use t_P^*, compute PREM travel times and ray paths for P waves, and relate Q_P to Q_μ via Eq. (5).

We impose smoothness to the Q_μ structure by penalizing differences in Q_μ for nearby layers:

$$W_{ij}\left(\frac{1}{Q_\mu^i} - \frac{1}{Q_\mu^j}\right) = 0, \tag{14}$$

where

$$W_{ij} = \exp\left\{-\left(\frac{i-j}{5}\right)^2\right\}, \tag{15}$$

and i and j are layer indices. This constraint suppresses small-scale (< 150 km) depth variations of Q_μ.

We combine Eqs. (12), (13), and (14) to get a matrix-vector relationship $\mathbf{Gm} = \mathbf{d}$, akin to Section 3, where

$$\mathbf{m} = \left(\frac{1}{Q_\mu^1}, \frac{1}{Q_\mu^2}, \cdots, \frac{1}{Q_\mu^N}\right). \tag{16}$$

and estimate $\mathbf{m}$ by least squares inversion.

4.1. Global variation of Q_μ

The best-fitting Q_μ profile is shown in Fig. 6 and Table 1. The Q_μ profiles from PREM, QL6, and QLM9 are shown for comparison. The structure of Q_μ has minima and maxima that track the maxima and minima t_P^* and t_S^*. Given the large scatter of the body-wave spectra and, consequently, the large uncertainties in t_P^* and t_S^*, we emphasize

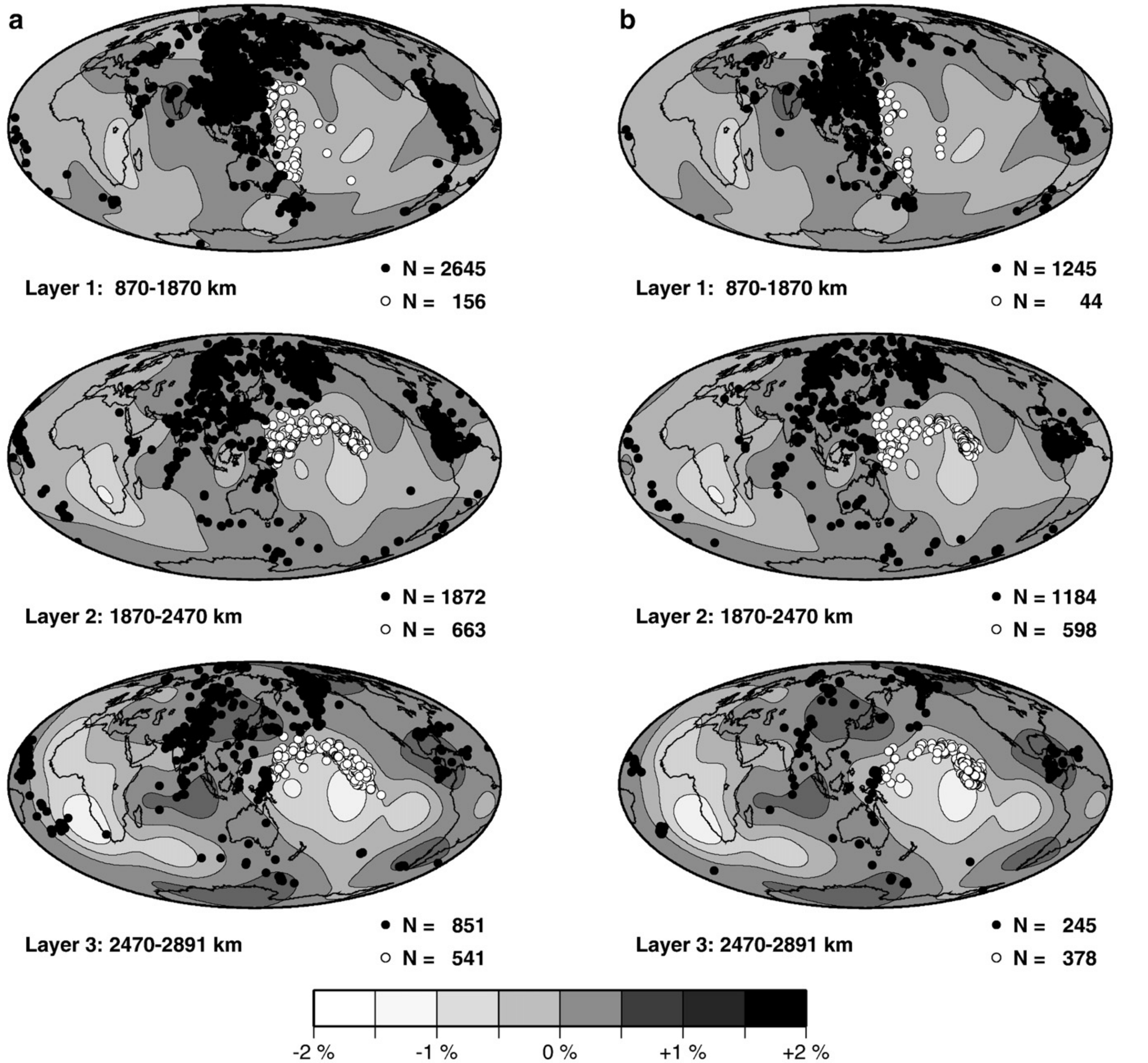

Fig. 5. Turning points of (a) P and (b) S waves used in this study within (top) Layer 1 (870–1870 km), (middle) Layer 2 (1870–2470 km), and (bottom) Layer 3 (2470–2891 km). The number of turning points for the Pacific group (white circles) and the circum-Pacific group (black circles) groups are indicated below the maps. The background represents the shear velocity variation (plotted up to degree 8) at depths of 1500 km, 2100 km, and 2700 km according to S20RTS (Ritsema et al., 1999).

only the increasing values of Q_μ with depth as the robust model feature. Q_μ increases from 360 at the 670-km discontinuity to a maximum value of 670 just above the CMB. It increases, on average, by about 0.12 km^{-1} between 1000 and 2500 km depth in contrast to the 0.09 km^{-1} rate of increase of Q_μ in QLM9. The relatively strong increase of Q_μ is linked to the relatively modest increase of t_P^* and t_S^* compared to PREM, QL6, and QLM9 (Fig. 4). The mean value of Q_μ model in the lower mantle is about 520 which is 45% and 65% larger than Q_μ in QL6 and PREM, respectively.

4.2. Pacific and circum-Pacific Q_μ structure

Fig. 6 shows profiles of Q_μ inferred from the complete (i.e., global) data set and the Pacific and circum-Pacific subsets as defined in Section 3.2. The contrast between the Pacific and circum-Pacific Q_μ structure is best resolved in layer 2 (1870–2470 km depth). Here, Q_μ beneath the Pacific is 520 on average in contrast to the circum-Pacific average Q_μ value of 560. Therefore, it appears that Q_μ in the lower mantle beneath the Pacific, which is characterized by a large-scale shear-velocity reduction of 1–3%, is smaller roughly by 10% (17% at most at a depth of about 2100 km) than in the circum-Pacific region.

5. Discussion and conclusions

In this paper we have applied a multi-taper analysis to examine nearly 300,000 ratios of broadband P and S wave spectra. We determine the P-wave and S-wave body-wave attenuation parameters t_P^* and t_S^* and a radial profile of Q_μ for the lower mantle. Despite significant measurement scatter we observe that t_P^* and t_S^* increase by about 0.2 s and 0.7 s, respectively, between epicentral distances of 30° and 97°. The t_P^* increase of 0.2 s is comparable to the difference in spatial t_P^* of 0.2 s between tectonically active western North America and stable eastern North America (Hwang et al., 2009).

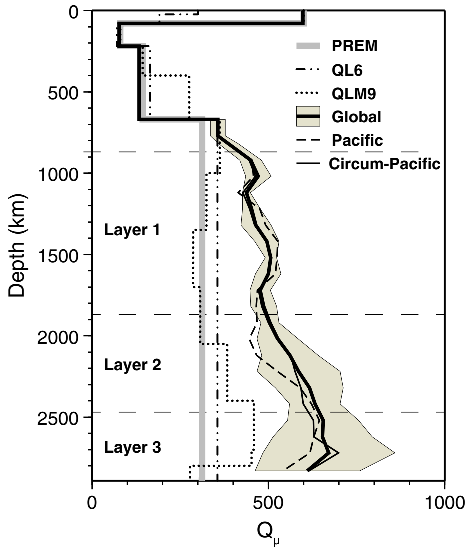

Fig. 6. Radial variation of Q_μ for complete (Global) data (thick black lines) with its error (shaded area), the Pacific group (dashed lines), and the circum-Pacific group (thin black lines), which are compared with Q_μ profiles from PREM (thick gray lines), QL6 (two-dot chain lines), and QLM9 (dashed dotted lines). Horizontal dashed lines represent the boundaries between Layer 1, Layer 2, and Layer 3.

Thus, the dependence on distance cannot be neglected when estimating spatial variations of t_P^* and t_S^*.

The t_S^*/t_P^* ratio is about 4, which is consistent with the common observation that attenuation in the bulk modulus is negligible compared to attenuation in the shear modulus since attenuation occurs mostly in shear (e.g., Anderson and Given, 1982). It is also consistent with the ratio between t_P^* (~1 s) and t_S^* (~4 s) estimated from spectral and time-domain body-wave studies (see the review by Cormier (1982)).

The increase of t_P^* and t_S^* with distance is smaller than predicted by profiles of Q_μ derived from normal-mode data. This implies that the quality factor Q_μ in the lower mantle is not constant (as in PREM and QL6) or decreasing (as in PAR3P, QM1, or in Resovsky et al., (2005))for body waves at a period of about 1 s. Rather, it can only be explained if Q_μ increases with depth with a rate of about 0.12 km^{-1}. The increase is 40% larger than in model QLM9, which is derived from long-period S and ScS waveforms, although the gradient of Q_μ in QLM9 in the lowermost 1000 km of the mantle is consistent with our data.

Since Q_μ in the upper mantle cannot be constrained from our Δt^* measurements, we assume PREM's Q_μ structure for the upper mantle. Under this assumption, Q_μ is, on average, 516 in the lower mantle which is larger than Q_μ in PREM and QL6 by about a factor of 1.5. Frequency-dependence of Q_μ in the form of $Q=Q_0\,\omega^\alpha$ can explain the difference between the PREM Q_μ value (312 in the lower mantle) and the average Q_μ value (516) constrained here if $\alpha\approx0.1$, which is within the range of values obtained theoretically (e.g., Minster and Anderson, 1981) and from seismological observations (e.g., Anderson and Given, 1982; Lekić et al., 2009; Shito et al., 2004; Smith and Dahlen, 1981).

Table 1
The profile of the best-fitting Q_μ model as a function of depth (km).

Depth (km)	Q_μ	Depth (km)	Q_μ
770	356	1820	486
820	386	1920	504
920	449	2020	526
1020	471	2120	561
1120	437	2220	585
1220	451	2320	616
1320	464	2420	631
1420	495	2520	655
1520	507	2620	653
1620	495	2720	671
1720	476	2820	610

We estimate Q_P and Q_μ models separately by using, respectively, P wave and S wave data to determine the Q_P/Q_μ ratio for our data and investigate the effect of finite Q_κ. The Q_P/Q_μ ratio for our Q_P and Q_μ models in the lower mantle is about 2.27 on average. This ratio is almost the same as the Q_P/Q_μ of 2.25 when $Q_\kappa^{-1}=0$ is assumed. This shows that our individual Q_P and Q_μ estimates are reasonable because intrinsic seismic attenuation occurs mostly in shear and the bulk attenuation in negligible, i.e., $Q_\mu \ll Q_\kappa$ (Anderson and Given, 1982).

Roth et al. (1999) suggested that the loss in bulk can be as high as one third of the loss in shear which is equivalent to Q_P/Q_μ ratio as low as 1.75. In order to investigate the effect of a finite Q_κ value, we invert for Q_μ using Eq. (4) and a Q_P/Q_μ ratio of 1.75. This results in a Q_μ decrease of about 15% between 670 and 1500 km depth but Q_μ decreases by less than 5% in the lower half of the mantle (>1500 km depth). In addition, the increase of Q_μ with depth remains evident. When only P waves are used to invert for radial Q_P model, our Q_P increases from about 820 at 670 km depth to its maximum value of about 1450 at 2700 km depth. The mean value of our Q_P in the lower mantle is about 1110. This is about 40% larger than the average Q_P in the lower mantle in PREM (about 780) but about 60% smaller than the Q_P value in the lower mantle (about 2600) according to (Warren and Shearer, 2000) which is measured at relatively high frequencies between 0.16 and 0.86 Hz.

We have explored whether lateral variations in t_P^*, t_S^* and Q_μ are resolvable by dividing the data set in two subsets that are defined by tomographic maps of shear velocity. The Pacific subset includes body-wave spectra associated with P and S wave turning points in the lower mantle beneath the Pacific Ocean, where shear velocities are relatively low. The circum-Pacific subset includes body-wave spectra with P and S waves that turn in higher-than-average shear velocity regions of the lower mantle. Between epicentral distance of 70° and 85°, when the measurements are most abundant, t_P^* and t_S^* for the Pacific subset is larger than for the circum-Pacific subset.

Q_μ beneath the Pacific is, on average, 520 between 1870 and 2470 km depth. In contrast, Q_μ determined for the circum-Pacific data is, on average, 560 between 1870 and 2470 km depth, similar to what is resolved for the complete data set. Therefore, we find that Q_μ is reduced within the large-scale low-velocity province of the lower mantle beneath the Pacific. If this difference is representative of the large-scale variations of Q_μ in the lower mantle, we place an upper limit to Q_μ variations of about 17%. Due to the interference of P and S and the core-reflections PcP and ScS, t_P^* and t_S^* for distances larger than 85° may be inaccurate. Consequently, Q_μ cannot be constrained for depths larger than about 2500 km, including the D'' layer.

Acknowledgments

This research has been funded by NSF grant EAR–0944167. Data have been provided by the IRIS/DMD and the Geoscope Data Center. Figures have been produced using the GMT software of (Wessel and Smith, 1995). We thank the reviewers for constructive reviews.

References

Anderson, D.L., Given, J.W., 1982. Absorption band Q model for the Earth. J. Geophys. Res. 87, 3,893–3,904.
Baqer, S., Mitchell, B.J., 1998. Regional variation of Lg coda Q in the continental United States and its relation to crustal structure and evolution. Pure Appl. Geophys. 153, 613–638.
Bhattacharyya, J., Masters, G., Shearer, P., 1996. Global lateral variations of shear wave attenuation in the upper mantle. J. Geophys. Res. 101, 22,273–22,289.

Billien, M., Lévêque, J.J., Trampert, J., 2000. Global maps of Rayleigh wave attenuation for periods between 40 and 150 seconds. Geophys. Res. Lett. 27, 3,619–3,622.
Booth, D.C., Marshall, P.D., Young, J.B., 1974. Long and short period P-wave amplitudes from earthquakes in the range 0°–114°. Geophys. J. R. Astron. Soc. 39, 523–537.
Butler, R., Ruff, L., 1980. Teleseismic short-period amplitudes, source and receiver variations. Bull. Seismol. Soc. Am. 70, 831–850.
Cormier, V.F., 1982. The effect of attenuation on seismic body waves. Bull. Seismol. Soc. Am. 72, S143–S173.
Dalton, C.A., Ekström, G., Dziewonski, A.M., 2008. The global attenuation structure of the upper mantle. J. Geophys. Res. 113, doi:10.1029/2007JB005429.
Der, Z.A., McElfresh, T.W., 1977. The relationship between anelastic attenuation and regional amplitude anomalies of short-period P waves in North America. Bull. Seismol. Soc. Am. 67, 1,303–1,317.
Der, Z.A., McElfresh, T.W., O'Donnell, A., 1982. An investigation of the regional variations and frequency dependence of anelastic attenuation in the mantle under the United-States in the 0.5–4 Hz band. Geophys. J. R. Astron. Soc. 69, 67–99.
Durek, J.J., Ekström, G., 1996. A radial model of anelasticity consistent with long-period surface wave attenuation. Bull. Seismol. Soc. Am. 86, 144–158.
Dziewonski, A.M., Anderson, D.L., 1981. Preliminary reference Earth model. Phys. Earth Planet. Inter. 25, 297–356.
Gung, Y., Romanowicz, B., 2004. Q tomography of the upper mantle using three-component long-period waveforms. Geophys. J. Int. 157, 813–830.
Hwang, Y.K., Ritsema, J., Goes, S., 2009. Spatial variations of P wave attenuation in the mantle beneath North America. J. Geophys. Res. 114, doi:10.1029/2008JB006091.
Lawrence, J.F., Wysession, M.E., 2006a. QLM9; A new radial quality factor (Q_u) model for the lower mantle. Earth Planet. Sci. Lett. 241, 962–971.
Lawrence, J.F., Wysession, M.E., 2006b. Seismic evidence for subduction-transported water in the lower mantle. Earth's deep water cycle, Geophys. Monogr. AGU, pp. 251–261.
Lawrence, J.F., Shearer, P.M., Masters, G., 2006. Mapping attenuation beneath North America using waveform cross-correlation and cluster analysis. Geophys. Res. Lett. 33, L07315, doi:10.1029/2006GL025813.
Lees, J.M., Park, J., 1995. Multiple-taper spectral analysis; A stand-alone C-subroutine. Comp. Geosci. 21, 199–236.
Lekić, V., Matas, J., Panning, M., Romanowicz, B., 2009. Measurement and implications of frequency dependence of attenuation. Earth Planet. Sci. Lett. 282, 285–293.
Minster, J.B., Anderson, D.L., 1981. A model of dislocation-controlled rheology for the mantle. Phil. Trans. R. Soc. Lond. 299, 319–356.
Okal, E.A., Jo, B.G., 1990. Q measurements for phase X overtones. Pure Appl. Geophys. 132, 331–362.
Oki, S., Shearer, P.M., 2008. Mantle Q structure from S–P differential attenuation measurements. J. Geophys. Res. 113, doi:10.1029/2007JB005567.
Reid, F.J.L., Woodhouse, J.H., van Heijst, H.J., 2001. Upper mantle attenuation and velocity structure from measurements of differential S phases. Geophys. J. Int. 145, 615–630.
Resovsky, J., Trampert, J., van der Hilst, R.D., 2005. Error bars for the global seismic Q profile. Earth Planet. Sci. Lett. 230, 413–423.
Ritsema, J., van Heijst, H.J., Woodhouse, J.H., 1999. Complex shear velocity structure imaged beneath Africa and Iceland. Science 286, 1,925–1,928.
Romanowicz, B., 1995. A global tomographic model of shear attenuation in the upper mantle. J. Geophys. Res. 100, 12,375–12,394.
Roth, E.G., Wiens, D.A., Dorman, L.M., Hildebrand, J., Webb, S.C., 1999. Seismic attenuation tomography of the Tonga-Fiji region using phase pair methods. J. Geophys. Res. 104, 4,795–4,809.
Roth, E.G., Wiens, D.A., Zhao, D., 2000. An empirical relationship between seismic attenuation and velocity anomalies in the upper mantle. Geophys. Res. Lett. 27, 601–604.
Roult, G., Clévédé, E., 2000. New refinements in attenuation measurements from free-oscillation and surface–wave observations. Phys. Earth Planet. Inter. 121, 1–37.
Selby, N.D., Woodhouse, J.H., 2002. The Q structure of the upper mantle: constraints from Rayleigh wave amplitudes. J. Geophys. Res. 107, doi:10.1029/2001JB000257.
Sheehan, A.F., Solomon, S.C., 1992. Differential shear wave attenuation and its lateral variation in the north Atlantic region. J. Geophys. Res. 97, 15,339–15,350.
Shito, A., Karato, S., Park, J., 2004. Frequency dependence of Q in Earth's upper mantle inferred from continuous spectra of body waves. Geophys. Res. Lett. 31, doi:10.1029/2004GL019582.
Smith, M.L., Dahlen, F.A., 1981. The period and Q of the Chandler wobble. Geophys. J. R. Astron. Soc. 64, 223–281.
Solomon, S.C., Toksöz, M.N., 1970. Lateral variation of attenuation of P and S waves beneath the United States. Bull. Seismol. Soc. Am. 60, 819–838.
Stein, S., Wysession, M.E., 2003. An introduction to seismology, earthquakes, and Earth structure. Blackwell Publishing, Malden, MA.
Teng, T.L., 1968. Attenuation of body waves and the Q structure of the mantle. J. Geophys. Res., 73, pp. 2,195–2,208.
Warren, L.M., Shearer, P.M., 2000. Investigating the frequency dependence of mantle Q by stacking P and PP spectra. J. Geophys. Res., 105, pp. 25,391–25,402.
Warren, L.M., Shearer, P.M., 2002. Mapping lateral variations in upper mantle attenuation by stacking P and PP spectra. J. Geophys. Res. 107, doi:10.1029/2001JB001195.
Wessel, P., Smith, W.H.F., 1995. New version of the generic mapping tools released. EOS Trans. AGU 76, 329.
Widmer, R., Masters, G., Gilbert, F., 1991. Spherically symmetrical attenuation within the earth from normal mode data. Geophys. J. Int. 104, 541–553.